

Solvent-diluted Block Copolymers: Bulk and Interfacial Phenomena

Shai Cohen and David Andelman

*Raymond and Beverly Sackler School of Physics and Astronomy,
Tel Aviv University, Ramat Aviv, Tel Aviv 69978, Israel*

(Dated: submitted: July 21, 2013)

A phenomenological mean-field theory is used to investigate the properties of solvent-diluted di-block copolymers (BCP), in which the two BCP components (A and B) form a variety of phases that are diluted by a solvent (S). Using this approach, we model mixtures of di-block copolymers and a solvent, and obtained the three-component phase diagram and its critical behavior. In the low solvent limit, we find how the critical point depends on the solvent density. Due to the non-linear nature of the coupling between the A/B and BCP/solvent concentrations, the A/B modulation induces modulations in the polymer-solvent relative concentration with a double wavenumber. The free boundary separating the polymer-rich phase from the solvent-rich one is studied in two situations. First, we show how the presence of a chemically patterned substrate leads to deformations of the BCP film/solvent interface, creation of terraces in lamellar BCP film and even formation of multi-domain droplets as induced by the patterned substrate. Second, we compare the surface tension between parallel lamellae coexisting with a solvent phase with that of a perpendicular one, and show that the surface tension has a non-monotonic dependence on temperature. The anisotropic surface tension can lead to deformation of spherical BCP droplets into lens-shaped ones, together with re-orientation of the lamellae inside the droplet during the polymer/solvent phase separation process.

I. INTRODUCTION

A wide variety of chemical and physical systems exhibit patterns and textures are characterized by spatial modulations in thermodynamical equilibrium. Some of the most common morphologies are stripes and circular droplets in two dimensions (2D), as well as sheets, tubes and spherical droplets in three dimensions (3D). These systems are very diverse and include type I superconductor films, ferromagnetic films, diblock copolymers, and even lipid bio-membranes [1–3]. In each case the physical origin of the order parameter and pattern characteristic differs with length scales or periodicity that vary from mesoscopic scales of tens of nanometers in biological membranes [4], to centimeters in ferrofluids [2, 3]. The fact that such a vast variety of physical, chemical, and biological systems display morphological similarities, irrespective of the details of microscopic structure and interactions, is striking and can be explained by a generic mechanism of competing interactions [1–3].

A Ginzburg-Landau (GL) expansion [5] applicable to modulated phases was introduced [6] by adding to the free energy a term preferring a specific wavelength q_0 :

$$\frac{1}{2} \int \left[(\nabla^2 + q_0^2) \phi \right]^2 d^2r. \quad (1)$$

This positive-definite form is known as the Brazovskii form [6–11] and has a minimum at q_0 . Close to the critical point it has been shown by Brazovskii [6] and Leibler [7] that the amplitude of the most dominant q -mode, q_0 , grows much faster than other q -modes. This form and similar ones have been used to calculate phase diagrams and grain boundaries of modulated phases [12–14], as well as to study the effects of chemically patterned surfaces on such phases [15–19]. In particular, such coarse-

grained models compare well with experimental phase diagrams [20] and with grain boundaries of block copolymers (BCP) [21–23].

In the present study we consider an extension of modulated phases that are diluted by a solvent. Although our phenomenological approach can apply to any modulated phase, we apply it explicitly to di-BCP diluted by a solvent in a variety of solvent conditions [24]. We investigate, in particular, bad solvent conditions where the phase separation between BCP and solvent allows us to explore the free interface between the BCP film and the bad solvent (vapor). Our study is relevant to a large number of experimental situations where a BCP film is spin casted on a solid substrate [25–35]. As the solvent evaporates, the polymer/air free interface can deform, and the free interface self-adjust its shape in order to minimize the total free energy. Another implication of our study is to experiments on BCP domain shapes and orientation of anisotropic phases within such domains, during phase separation between the polymer and a bad solvent.

The outline of our paper is as follows. In the next section we present our model, which is a generalization of phenomenological free-energy expansions used to model di-BCP systems. The free energy includes additional terms depending on the solvent (S) and its coupling with the A/B relative composition. In section III we present the bulk properties of the ternary solvent-BCP system, including the global phase diagrams, an explanation of the period-doubling phenomena found for the polymer density, and an analysis of the critical point in the low-solvent limit. In section IV, we present results for grain boundaries between lamellar domains of different orientations and the interface structure of coexisting hexagonal and disordered phases. In section V we show how a chemically patterned substrate influences deformations of

a flat free interface and formation of BCP droplets, while in section VI we study the temperature dependence of the surface tension between lamellar and solvent phases, for parallel and perpendicular orientations. We also show in section VI how such an anisotropic surface tension affects the shape of circular lamellar drops of BCP during the overall solvent/polymer phase separation process.

II. THE FREE ENERGY OF SOLVENT – BCP MIXTURES

In this study we employ a phenomenological free-energy of mixing [36, 37] of a ternary mixture composed of three components: A, B and S. The A and B components are the two component of a di-BCP [12] and have volume fractions ϕ_A and ϕ_B , while S is a solvent with volume fraction ϕ_S . All three volume fractions satisfy $0 \leq \phi_i \leq 1$, $i = A, B, S$.

Using the incompressibility condition

$$\phi_A + \phi_B + \phi_S = 1, \quad (2)$$

it is more convenient to consider the two following order-parameters:

$$\begin{aligned} \rho &= \phi_A + \phi_B, \\ \phi &= \phi_A - \phi_B, \end{aligned} \quad (3)$$

where $0 \leq \rho \leq 1$ is the solute (BCP) volume fraction and $-1 \leq \phi \leq 1$ is the relative A/B concentration of the two blocks, satisfying $|\phi| \leq \rho$.

We work in the grand-canonical ensemble where the Gibbs free-energy density (per unit volume) g is defined as

$$g = \varepsilon - Ts - \sum_{i=A,B,S} \mu_i \phi_i, \quad (4)$$

with ε being the enthalpy, $s = -k_B \sum_i \phi_i \ln(\phi_i)$ the ideal entropy of mixing, and μ_i the chemical potential of the i -th species. Writing ε in terms of all two-body interactions between the three components, and expressing the free-energy g in terms of the ρ and ϕ densities, yields

$$\begin{aligned} \frac{g(\phi, \rho)}{k_B T} &= -\frac{\tau}{2} \phi^2 + \frac{\chi}{2} \rho(1 - \rho) + v_{\phi\rho} \phi(1 - \rho) - \mu_\phi \phi - \mu_\rho \rho \\ &+ \frac{\rho + \phi}{2} \ln(\rho + \phi) + \frac{\rho - \phi}{2} \ln(\rho - \phi) \\ &+ (1 - \rho) \ln(1 - \rho) + \frac{H}{2} \left[(\nabla^2 + q_0^2) \phi \right]^2 \\ &+ K(\nabla \rho)^2, \end{aligned} \quad (5)$$

where τ is the interaction parameter between the A and B monomers of the BCP, χ is the solvent-polymer interaction parameter, and $v_{\phi\rho}$ is the parameter denoting any asymmetry in the interaction between the solvent and the A and B components. The next two terms are the chemical potential ones, where μ_ϕ couples linearly to ϕ and

μ_ρ to the polymer volume fraction ρ , and the three logarithmic terms originate from the ideal entropy of mixing. So far the terms of g describe any three-component mixture of A, B and S within the ideal solution (mean-field) theory. In order to model the A/B mixture as a di-BCP, we add to eq 5 the H -term as introduced in eq 1, where H is the modulation coefficient and q_0 is the most dominant wavevector [6–13]. As we are interested in studying interfacial phenomena between polymer-rich and solvent-rich phases, we also included a gradient squared term in the polymer density ρ to account for the cost of density fluctuations, where $K > 0$ is a measure of the interface “stiffness” [38].

The free energy of eq 5 can be reduced to several simple limits. (i) For $\rho = 1$, the system reduces to the pure A/B di-BCP. Here $\phi_S = 0$ and

$$\begin{aligned} \frac{g}{k_B T} &= -\frac{\tau}{2} \phi^2 + \frac{1 + \phi}{2} \ln(1 + \phi) + \frac{1 - \phi}{2} \ln(1 - \phi) \\ &+ \frac{H}{2} \left[(\nabla^2 + q_0^2) \phi \right]^2 - \mu_\phi \phi. \end{aligned} \quad (6)$$

This case was mentioned in section I and has been studied extensively in the past [6, 7]. The BCP phase has a critical point at $\tau_c = 1$ and for $\tau > \tau_c$, only the disordered phase is stable. (ii) Another simple limit is obtained by setting $\phi = \phi_A - \phi_B = 0$, yielding

$$\begin{aligned} \frac{g}{k_B T} &= K(\nabla \rho)^2 + \frac{\chi}{2} \rho(1 - \rho) + \rho \ln \rho \\ &+ (1 - \rho) \ln(1 - \rho) - \mu_\rho \rho. \end{aligned} \quad (7)$$

This is the free energy of a solvent/solute binary mixture, where ρ is the solute volume fraction [36]. In the bulk, $\rho = \text{const.}$, and one gets a demixing curve between two macroscopically separated phases. The demixing curve terminates at a critical point located at $\chi_c = 4$ and $\rho_c = 0.5$.

III. BULK PROPERTIES

A. Global Phase Diagrams

The equilibrium phases are found by minimizing numerically the free energy given by eq 5, using periodic boundary conditions on our simulation box. We will consider hereafter only symmetric interactions of the A and B components with the S solvent. Hence, we set $v_{\phi\rho} = 0$ throughout the remainder of the paper. In addition, all numerical calculations are restricted to two dimensions (2d) so that only lamellar and hexagonal phases are considered and not three-dimensional phases of cubic symmetry, such as BCC and gyroid phases. We do not vary the values of q_0 , H and K but set their values to: $q_0 = 1/\sqrt{2}$, $H = 1$ and $K = 1$. We are left with two interaction parameters τ and χ and two chemical potentials μ_ϕ and μ_ρ that determine the bulk (average) densities, $\phi_0 = \langle \phi \rangle$ and $\rho_0 = \langle \rho \rangle$. In figure 1 (a), (c)

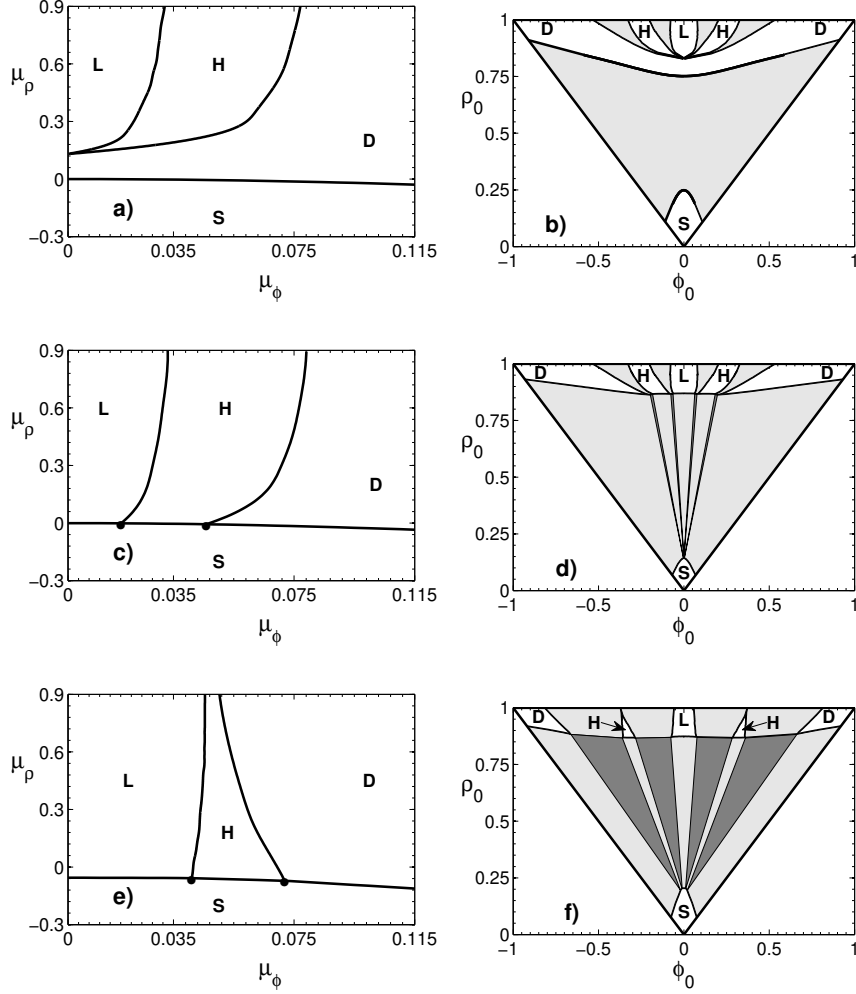


FIG. 1: Phase diagrams plotted for $H = K = 1$ and $v_{\phi\rho} = 0$, in the chemical potential (μ_ρ, μ_ϕ) plane on the left panels and in the density (ρ_0, ϕ_0) plane on the right panels. The various phases are denoted as: D (disorder), L (lamellar), H (hexagonal) and S (solvent-rich). In (a) and (b) $\chi = 4.4$ and $\tau = 1.2$, and the solvent-solute phase separation occurs only in the disordered phase, resulting in an S-D coexistence regions. In (c) and (d), $\chi = 5$ and $\tau = 1.2$, and the increase of χ results in D-S, H-S and L-S coexistence regions. In addition, three-phase coexisting regions start to emerge (marked by dark gray). In (e) and (f), $\chi = 4.4$ and $\tau = 1.6$, and the increase of τ causes a near disappearance of the H phase and more extended three-phase coexistence regions.

and (e), we plot cuts of the phase diagram for several values of χ and τ in the (μ_ϕ, μ_ρ) plane, while in parts (b), (d) and (f), the corresponding phase diagrams are shown in the density plane (ϕ_0, ρ_0) , where the phase diagrams are triangular due to the incompressibility condition $0 \leq |\phi_0| \leq \rho_0 \leq 1$. Note that the phase diagrams are symmetric around $\phi_0 = 0$ and $\mu_\phi = 0$, because we restrict ourselves to the $v_{\phi\rho} = 0$ symmetric case.

The phase diagrams in figure 1 display regions of a single phase marked as D (disorder), L (lamellar), H (hexagonal) or S (solvent-rich). Between these single-phase regions there are two-phase (light gray) and three-phase (dark gray) coexisting regions. Both D and S phases are homogenous liquid-like phases with no modulation. The S phase is richer in the solvent, whereas the D one in the

solute (i.e., polymer). Within the single q -mode approximation the various phases (restricted to 2d systems) are expressed as:

$$\begin{aligned} \phi_D &= \phi_0, \\ \phi_S &= \phi_0, \\ \phi_L &= \phi_0 + \phi_q \cos(q_0 x), \\ \phi_H &= \phi_0 + \sum_{i=1}^3 \phi_q \cos(\mathbf{q}_i \cdot \mathbf{r}); \quad \sum_{i=1}^3 \mathbf{q}_i = 0. \end{aligned} \quad (8)$$

The hexagonal phase is composed of three q -vectors in the (x, y) plane, $|\mathbf{q}_i| = q_0$.

To see how the changes in χ and τ affect the phase diagram, let us first examine figure 1(a) and (b). These figure parts show the phase diagram for $\chi = 4.4$ and

$\tau = 1.2$, plotted in the (μ_ρ, μ_ϕ) plane in (a), and the (ρ_0, ϕ_0) plane in (b). For these specific parameter values there are no coexistence regions between the solvent-rich and BCP phases, because the D-S and H-D lines do not intersect [figure 1(a)]. In order to have a coexistence region between modulated and solvent phases, one must induce the solute-solvent phase-transition to occur before the BCP phase ceases to exist. This is achieved for larger values of $\chi = 5$ in figure 1(c) and (d), while keeping $\tau = 1.2$. The solvent-solute coexistence region is bigger than in 1(a), allowing L-S and H-S coexisting regions, in addition to the D-S region of figure 1(a). Moreover, three-phase coexisting regions start to emerge. Next, the effect of increasing τ is shown in figure 1(e) and (f) with $\tau = 1.6$. As τ becomes bigger, the BCP phases endure smaller values of ρ_0 , in such a way that the extent of two- and three-phase coexistence regions increases.

B. The low solvent limit and its critical behavior

Since our free energy reduces to eq 6 for $\rho = 1$ (no solvent), a BCP phase for the A/B system exists for $\rho = 1$ as long as $\tau > \tau_c$, where $\tau_c = 1$ is the critical point. To gain some insight of the behavior for the ternary system, $\rho_0 < 1$, we plot a typical free-energy landscape corresponding to the disordered phase in figure 2. In figure 2(a), $\tau = 1.45$ is above the critical point, $\tau_c = 1$, and the disordered phase is not stable. Instead, we notice three local minima denoted by A, B and S. The A and B minima denote two equivalent points for which the solute density is high ($\rho_0 \approx 0.9$) and is composed mainly of the A component ($\phi_0 \approx 0.3$) or the B component ($\phi_0 \approx -0.3$). Point S, on the other hand, has low solute density ($\rho_0 \approx 0.2$) and is composed of an equal amount of the A and B ($\phi_0 = 0$). In addition, note also that the energy is concave on the $\rho_0 = 1$ line.

Figure 2(a) should be compared with 2(b), for which $\tau = 0.5 < \tau_c = 1$. In this case, only two minima exist and are denoted as S (solvent rich as before) and D (disorder solute-rich). For the D minimum the concentration ρ_0 is high and equal amounts of A and B component are present ($\phi_0 = 0$). The free energy is convex on the $\rho_0 = 1$ line. We conclude that modulations can only occur if the A and B minima exist so that the two component tend to separate, while the modulation term dictates the length scale of spatial modulations by having the ϕ composition oscillates between these two states. Looking at figure 2(a) along the symmetric $\phi_0 = 0$ line, we further remark that the free energy changes from being slightly concave at $\rho_0 \lesssim 1$ to highly convex close to $\rho_0 = 0$. This change in convexity suggests that a lamellar phase in ϕ will only be energetically favorable at $\rho_0 \simeq 1$, because in the highly convex region only one minimum exists. It also suggests that the critical point τ_c will grow as ρ_0 decreases.

We would like next to obtain an analytical expression of $\tau_c(\rho)$, for $\rho \lesssim 1$, while recalling that without any solvent, $\tau_c(\rho=1) = 1$. We use the lamellar single-mode ap-

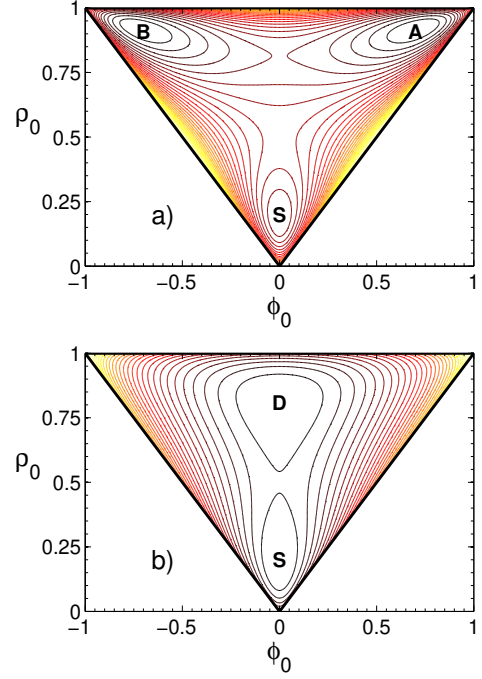


FIG. 2: (colored online) The free-energy landscape obtained from the contour plot of the ternary-mixture free energy, eq 5, disregarding the spatially varying terms, for $\chi = 4.4$ and $\mu_\rho = \mu_\phi = 0$. In (a) $\tau = 1.45 > \tau_c$ while in (b) $\tau = 0.5 < \tau_c$. The free-energy minima are denoted by A, B and S and (a) and D and S in (b).

proximation, and expand the free energy in powers of ϕ/ρ . Because $|\phi| < \rho$, ϕ/ρ may serve as a small expansion parameter around the ($\rho \simeq 1$, $\phi = 0$) corner of the phase diagram. Expanding the entropy in eq 5 to fourth order in ϕ/ρ results in:

$$\begin{aligned} \frac{g}{k_B T} \simeq & -\frac{\tau}{2}\phi^2 + \frac{\chi}{2}\rho(1-\rho) + (1-\rho)\ln(1-\rho) + \rho\ln\rho \\ & + \frac{\phi^2}{2\rho} + \frac{\phi^4}{12\rho^3} + \frac{H}{2}\left[(\nabla^2 + q_0^2)\phi\right]^2 \\ & + K(\nabla\rho)^2 - \mu_\rho\rho - \mu_\phi\phi. \end{aligned} \quad (9)$$

Since the only source of modulations is the $\frac{H}{2}[(\nabla^2 + q_0^2)\phi]^2$ term, modulations in ρ can be induced by modulations in ϕ through an entropy-mediated interaction, as will be explain in detail in section III.C below. Thus, it is reasonable to assume that close to the critical point, where ϕ starts to modulate, the modulations in ρ are small and their effect on the ϕ modulations can be neglected (to be further justified below).

Dropping the constant terms in ρ from eq 9 yields,

$$\frac{g}{k_B T} = -\frac{\tau}{2}\phi^2 + \frac{\phi^2}{2\rho} + \frac{\phi^4}{12\rho^3} + \frac{H}{2}\left[(\nabla^2 + q_0^2)\phi\right]^2. \quad (10)$$

Assuming for simplicity 1d lamellar modulations, we use for ϕ the single-mode ansatz $\phi(x) = \phi_0 + \phi_q \cos(q_0 x)$,

where $\phi_0 = \langle \phi \rangle$ is the spatial average of $\phi(x)$ and ϕ_q is its modulation amplitude, while $\rho(x)$ is taken without any spatial modulations and is equal to its special average, $\rho_0 = \langle \rho \rangle$ [39–42]. Taking a variation with respect ϕ_q , it can be shown that for the most dominant mode $q = q_0$, its amplitude ϕ_q satisfies:

$$\phi_q^2 = 4\rho_0^3 \left(\tau - \frac{\phi_0^2}{\rho_0^3} - \frac{1}{\rho_0} \right). \quad (11)$$

From eq 11, we get a condition for the extent of the lamellar phase by requiring that $\phi_q^2 \geq 0$, and the critical temperature is obtained at $\phi_q = 0$:

$$\tau_c = \phi_0^2 / \rho_0^3 + 1 / \rho_0. \quad (12)$$

For symmetric lamellae, where $\phi_0 = 0$, we get $\tau_c = 1 / \rho_0$ that agrees with $\tau_c = 1$ for $\rho_0 = 1$. Furthermore, for $\rho_0 \rightarrow 0$ we get $\tau_c \rightarrow \infty$ implying that the only possible phase at low solute concentrations is the disordered phase. Substituting eq 11 into eq 9 gives (within the single-mode approximation) the lamellar free-energy as a function of ϕ_0 :

$$\frac{g_L}{k_B T} = \frac{1}{2} \left(\tau - \frac{1}{\rho_0} + H q_0^4 \right) \phi_0^2 - \frac{5\phi_0^4}{12\rho_0^3} - \frac{\rho_0^3}{2} \left(\tau - \frac{1}{\rho_0} \right)^2. \quad (13)$$

This lamellar (L) phase exists as long as $\phi_0^2 \leq \tau \rho_0^3 - \rho_0^2$ [from eq 11], and its free energy can be compared with that of the disordered (D) phase:

$$\frac{g_D}{k_B T} = \frac{1}{2} \left(\frac{1}{\rho_0} + H q_0^4 - \tau \right) \phi_0^2 + \frac{\phi_0^4}{12\rho_0^3}. \quad (14)$$

The minimum of the D phase is located at

$$\phi_0 = \sqrt{3\rho_0^3(\tau - 1/\rho_0 - H q_0^4)}, \quad (15)$$

and the free energy at this minimum is

$$\frac{g_D}{k_B T} = -\frac{2\rho_0^3}{3} (\tau - 1/\rho_0 - H q_0^4)^2. \quad (16)$$

The minimal free energy of the L phase occurs at $\phi_0 = 0$, giving

$$\frac{g_L}{k_B T} = -\frac{\rho_0^3}{2} (\tau - 1/\rho_0)^2. \quad (17)$$

By equating the two free energies, we see that the D phase becomes more stable than the L phase for $\tau \geq H q_0^4 / (1 - \sqrt{3/4}) + 1/\rho_0$. Thus, yielding the termination of the L phase at a triple point, $\tau_{\text{tri}} = H q_0^4 / (1 - \sqrt{3/4}) + 1/\rho_0$. This termination is similar to the one described in ref [12], but is not necessarily experimentally feasible, because in experiments other phases with 2d or 3d morphologies may pre-empt this phase behavior (see refs [41, 42] for more details). The above derivation also allows us to find an estimate for the tricritical point (tcp) by examining the change in convexity of the lamellar phase on the spinodal line ($\partial^2 g_L / \partial^2 \phi|_{\phi_q=0} = 0$), giving

$$\tau_{\text{tcp}} = H q_0^4 / 4 + 1/\rho_0. \quad (18)$$

C. Induced period doubling in ρ

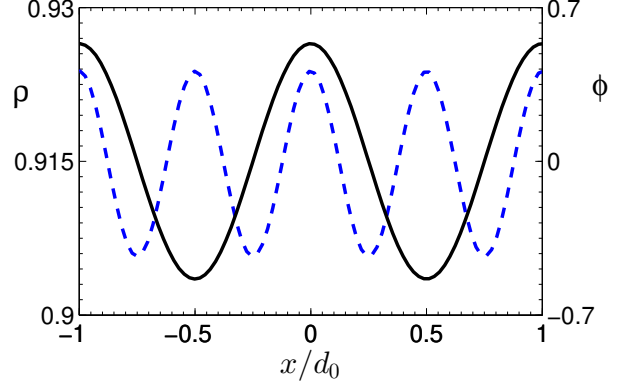


FIG. 3: (colored online) The spatial modulation of ρ (dashed line) and ϕ (solid line) are plotted as function of x/d_0 , with $d_0 = 2\pi/q_0$. The parameter values: $\tau = 1.2$, $\chi = 5.5$, $\mu_\phi = 0$ and $\mu_\rho = 0$ result in $\langle \rho \rangle = 0.915$ and $\langle \phi \rangle = 0$. The oscillations in ρ have half the wavelength of the ϕ ones. The length scale of the ρ modulations ($\rho_q = 0.0091$) is much smaller than the ϕ ones ($\phi_q = 0.538$).

The modulations in ϕ cause the overall BCP density, ρ , to modulate as well. Interestingly, the modulations in ρ are found to have half the wavelength of the ϕ modulations, and we would like to explain this period doubling phenomenon. In figure 3 such oscillations in ϕ and ρ can be clearly seen, where the amplitude of the ρ oscillations is much smaller than the ϕ ones. The reason for such oscillations is the nonlinear coupling between the ϕ and ρ order parameters, which has only entropic origin, as we restrict ourselves to the symmetric enthalpy case of $v_{\phi\rho} = 0$ in eq 5.

In figure 4 we show the contour plot of the free energy for $\chi = 4.2$ and $\tau = 1.45$. The spatial modulations in ϕ can be represented as an oscillatory path between the two free-energy minima denoted as A and B. The path between the two points will not take the direct route denoted by ‘1’ for which $\rho = \text{const.}$, but rather a curved and longer route denoted by ‘2’, because the latter is energetically preferred as it avoids the energy barrier along the direct path. Thus, oscillations in the ϕ order parameter induce oscillations in ρ . The fact that the ρ wavenumber is doubled ($2q_0$), as compared with the ϕ wavenumber (q_0), can also be understood from figure 4. For each cycle going from A to B and back, ϕ completes one cycle, while ρ completes two cycles. We note that increasing χ will cause these oscillations to decrease their magnitude as the potential well in the ρ direction moves to higher values of ρ and becomes deeper.

It is easier to present an explanation to the induced modulations along one spatial direction, taken to be the x -direction; namely, $\rho = \rho(x)$ and $\phi = \phi(x)$. An analytical (yet approximate) expression of the modulation

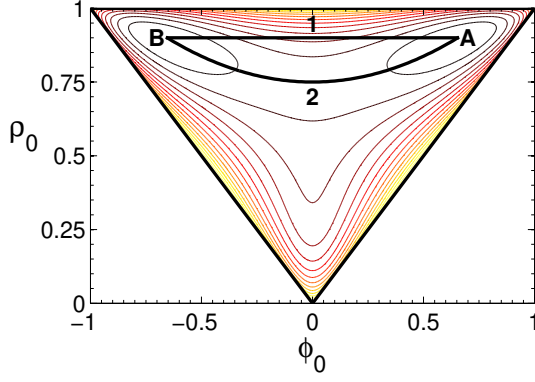


FIG. 4: (colored online) Two possible routes from point A to B, plotted on the free-energy contour plot in the (ϕ_0, ρ_0) plane, with $\chi = 4.2$, $\tau = 1.45$, $\mu_\rho = 0.05$ and $\mu_\phi = 0$. '1' is a straight route in which ρ does not change, while '2' is a curved one. The curved '2' path is energetically preferred as it bypasses the energy barrier along the direct '1' path between A and B.

amplitudes can be obtained by expanding the free energy, eq 9, in powers of $\eta(x) = \rho(x) - \rho_0$ around the value of the disordered phase, ρ_0 , to second order in ρ . Because the oscillations in ϕ are between two local minima in ϕ , we can further expand eq 9 to fourth order in ϕ :

$$\begin{aligned} \frac{g}{k_B T} \simeq & -\frac{\tau}{2}\phi^2 + \frac{\phi^2}{2\rho_0} + \frac{\phi^4}{12\rho_0^3} - \frac{\phi^2}{2\rho_0^2}\eta \\ & + \frac{1}{2}\left[\frac{1}{\rho_0} + \frac{1}{1-\rho_0} - \chi + \frac{\phi^2}{2\rho_0^3}\right]\eta^2 \\ & + K(\eta')^2 + \frac{H}{2}\left[\phi'' + q_0^2\phi\right]^2, \end{aligned} \quad (19)$$

where constant terms are omitted and ρ_0 is given by:

$$\frac{\chi}{2}(1 - 2\rho_0) + \ln \rho_0 - \ln(1 - \rho_0) - \mu_\rho = 0. \quad (20)$$

Taking the variation of g in eq 19 with respect to η and using the lamellar single-mode approximation, $\phi = \phi_q \cos(q_0 x)$ for symmetric lamellae, $\phi_0 = 0$, the inhomogeneous differential equation for $\eta(x) = \rho(x) - \rho_0$ is:

$$\begin{aligned} 2K\eta'' - \frac{1}{2}\left[\frac{1}{\rho_0} + \frac{1}{1-\rho_0} - \chi + \frac{\phi_q^2}{2\rho_0^3} + \frac{\phi_q^2}{2\rho_0^3}\cos(2q_0 x)\right]\eta \\ = -\frac{\phi_q^2}{4\rho_0^2}\left[1 + \cos(2q_0 x)\right], \end{aligned} \quad (21)$$

where the linear term in η originates from the quadratic term in the free energy. This term has to be positive because we have made an expansion around the free-energy minimum. This means that the homogenous solution of $\eta(x)$ is a decaying function and is of no interest, since we are only looking for periodic solutions of the bulk phases. The inhomogeneous solution $\eta(x)$, however, is caused by oscillatory cosine terms [RHS of eq 21]. To

obtain an approximate solution we take $\rho_0 \simeq 1$ and ϕ_q to be small, allowing us to neglect the sum of the two terms, $\phi_q^2(2\rho_0^3)^{-1} + \phi_q^2(2\rho_0^3)^{-1}\cos(2q_0 x)$, as compared with $(1 - \rho_0)^{-1}$. Then, eq 21 simplifies to:

$$\begin{aligned} 2K\eta'' - \frac{1}{2}\left[\frac{1}{\rho_0} + \frac{1}{1-\rho_0} - \chi\right]\eta \\ = -\frac{\phi_q^2}{4\rho_0^2}\cos(2q_0 x) - \frac{\phi_q^2}{4\rho_0^2}. \end{aligned} \quad (22)$$

By imposing a solution of the form $\eta = \eta_0 + \eta_{2q}\cos(2q_0 x)$ we get [43]:

$$\begin{aligned} \eta_0 &= \frac{\phi_q^2}{4\rho_0^2\varepsilon} \\ \eta_{2q} &= \frac{\phi_q^2}{4\rho_0^2(8Kq_0^2 + \varepsilon)}, \end{aligned} \quad (23)$$

where $\varepsilon = \rho_0^{-1} + (1 - \rho_0)^{-1} - \chi$. This solution makes sense as the modulations in ρ exist only when $\phi_q \neq 0$, and may appear at any ρ_0 , while larger densities or larger K values (high cost of the polymer/solvent interface) will make the modulations smaller. The fact that $\eta_0 \neq 0$ means that a lamellar modulating phase will cause an increase in the local solute density, recalling that $\eta_0 = \langle \eta \rangle$, is the spatial average of $\eta(x)$.

Comparison between the amplitude η_{2q} as obtained by solving numerically eq 5, and the approximated analytical one [using eqs 11 and 23] as a function of ρ_0 is shown in figure 5 for various τ values, where symmetric lamellae with $\phi_0 = 0$ are used. At small τ , the accuracy is very good since ϕ_q/ρ_0 is small. However, as τ grows so does ϕ_q , and the quality of the approximation deteriorates. Not surprisingly, as $\rho \rightarrow 1$, the modulations disappear. For large τ , the approximation worsens not only when ϕ_q is large, but also next to the critical density $\rho_c = 1/\tau$ when ρ becomes smaller.

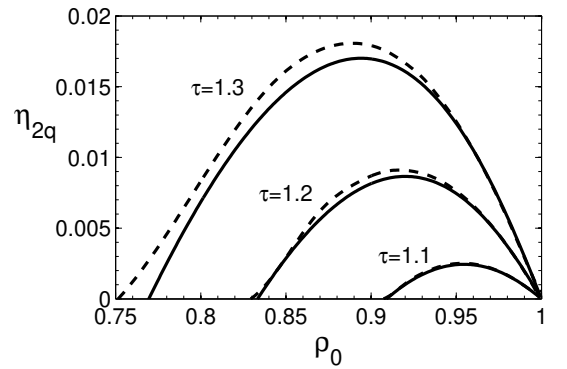


FIG. 5: Plot of η_{2q} as a function of ρ_0 for three values of $\tau = 1.1, 1.2, 1.3$, and with $\mu_\rho = \mu_\phi = 0$. The dashed line is the numerical solution of eq 5 and the solid line is the analytical approximation of eq 23.

IV. GRAIN BOUNDARIES AND INTERFACES

After constructing the global phase diagrams of the diluted BCP system, we study first the grain boundaries separating lamellar domains of different orientations, and then the interfaces between coexisting phases at equilibrium. The lamellar/lamellar grain boundary are obtained by minimizing numerically the free energy in a simulation box, with boundary conditions that are periodic on the vertical walls, while the top and bottom surfaces of the simulation box induce lamellar order with different orientations. Such 2D patterns in ϕ and ρ can be seen in figures 6 and 7. The left panels show the ϕ patterns, whereas the right panels show the corresponding ρ ones with a doubled wavenumber in their spatial periodicity, as was discussed in section III.C. Omega-shaped tilt grain boundaries (figure 6) and T-junction grain boundaries (figure 7) are shown as examples of possible grain boundaries between lamellar phases [12, 14]. Due to the wavenumber doubling effect one can see in both figures “bulbs” of higher density at the grain boundaries, which is more pronounced for the ρ patterns than for the ϕ ones. This is in agreement with experiments and calculations on blends of BCP and homopolymers showing that the homopolymer density is higher at the interfaces (e.g., T-Junction). This probably can be explained as a mechanism releasing some of the strain at the interface [44].

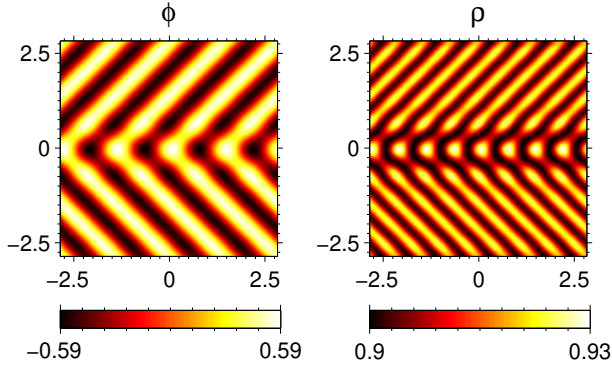


FIG. 6: (colored online) Omega-shaped grain boundary, also called “chevron”, between two lamellar grains that meet each other with a fixed angle. The angle is preset to be 90 degrees, and the parameter values are $\tau = 1.2$, $\mu_\rho = -0.004236$, $\chi = 5.5$ and $\mu_\phi = 0$. The axes are given in units of $d_0 = 2\pi/q_0$, and the color bar accounts for variation of each order parameter.

Since the wavenumber doubling phenomena is driven by entropy, it is not unique to the lamellar phase and can be obtained in other types of grain boundaries as well as interfaces between two coexisting phases at equilibrium. In figure 8 we present results for an interface between coexisting hexagonal and disordered phases at thermodynamical equilibrium. In the hexagonal phase the wavenumber doubling creates in ρ a pattern resem-

bling a “star of David”, and the decay of the ρ modulation into the D phase mimics that of the ϕ modulation. The length scale of the modulations does not seem to change while the modulation decay. By examining the interface between two coexisting phases, we note that the minimum of the free energy is obtained once the interface is flat, corresponding to an interface of minimal length. While patterns of pure BCP phases (the left panels representing the ϕ order parameter) have been explored extensively in the past [12–14], the addition of the solvent density and its oscillations with double periodicity is novel.

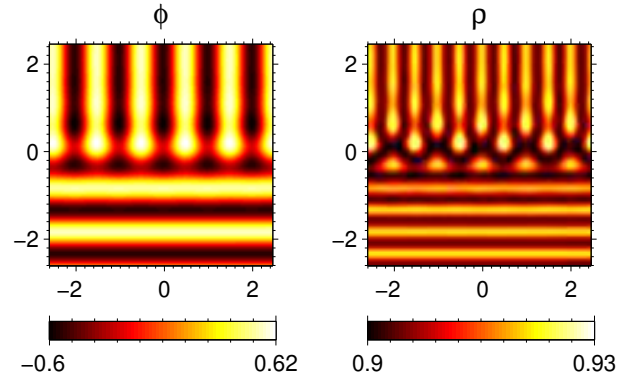


FIG. 7: (colored online) T-junction grain boundary between two perpendicular lamellar domains. The parameter values are $\tau = 1.2$, $\chi = 5.5$, $\mu_\rho = -0.004236$ and $\mu_\phi = 0$. The axes are given in units of $d_0 = 2\pi/q_0$, and the color bar accounts for variation of each order parameter.

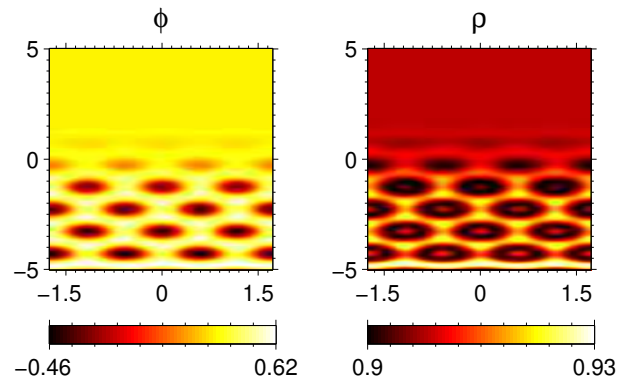


FIG. 8: (colored online) Interface between H (Hexagonal) and D (disordered) at coexistence. The parameter values are $\tau = 1.2$, $\chi = 5$, $\mu_\rho = 0.1842$, and $\mu_\phi = 0.0664$. The axes are given in units of $d_0 = 2\pi/q_0$, and the color bar accounts for variation of each order parameter.

V. SUBSTRATE CHEMICAL PATTERNING

Chemically and topographically patterned surfaces with preferential local wetting properties toward one of the two polymer blocks results in a unique organization of BCP thin films and have been investigated thoroughly in experiments [28–35]. We will explore here the interplay between such chemical heterogeneities on surfaces and the structure of BCP thin films.

A. Temporal evolution of lamellar ordering

Next we explore the effect of a chemically patterned surface on the BCP phase and its free interface. To see the effects rising from such a coupling, let us consider the temporal evolution of the minimization process. The initial guess for $-1 \leq \phi \leq 1$ is a random one where $\phi(\mathbf{r})$ is assigned a random initial value at each \mathbf{r} point, drawn from a uniform distribution with zero mean and standard deviation of 0.2. We use such a randomized initial guess because our model does not induce random fluctuations by itself. These fluctuations cause spontaneous symmetry breaking and spatial heterogeneity of the order parameter, and will allow the numerical procedure to converge towards the proper thermodynamical equilibrated state. A series of patterns is produced using eq 5 for which the lamellar phase is the equilibrium one.

The bulk BCP phase is placed in contact with a chemically patterned surface, modeled by two surface interactions: σ_ρ and σ_ϕ [11, 17], which are coupled linearly to ρ and ϕ , respectively. They lead to a new surface term G_s in the free energy

$$G_s = k_B T \int d^2 \mathbf{r}_s \left(\sigma_\rho(\mathbf{r}_s) \rho(\mathbf{r}_s) + \sigma_\phi(\mathbf{r}_s) \phi(\mathbf{r}_s) \right), \quad (24)$$

where \mathbf{r}_s is a vector on the 2-dim substrate. We first examine the effect of the patterned substrate on nucleation and orientation of an $L_{||}$ lamellar phase, and present the temporal evolution of such a phase in figure 9. The substrate is constructed in such a way that its field, σ_ϕ , prefers the B component in the surface mid-section, while it is neutral elsewhere:

$$\sigma_\phi = \begin{cases} 0.5 & |x| \leq 1.5d_0 \\ 0 & |x| > 1.5d_0 \end{cases} \quad (25)$$

In addition, the field σ_ρ is fixed to be zero on the entire substrate. The upper bounding surface is neutral, while the vertical walls obey periodic boundary conditions. During the early time stages, coarsening leads to density “lumps” ($t = 25$ and 100 where t indicates the simulation running steps), which then elongate to form several lamellar domains with different orientations ($t = 175$ and 700). As the minimization procedure continues, the direction parallel to the substrate ($L_{||}$) takes

over and becomes the dominant one ($t = 3016$). The quenched pattern on the substrate breaks the rotational symmetry and leads to nucleation of an $L_{||}$ phase around the mid-section of the surface. This surface effect propagates into the bulk as the simulation time t increases. At the final time step of figure 9 ($t = 3016$), the deformations of the lamellar structure due to the surface pattern are clearly seen close to the substrate and decays fast into the lamellar bulk [11].

B. The free interface

We can also address within our model and numerical scheme the *free interface* between a thin film of a lamellar BCP in coexistence with a bad solvent (vapor) [24, 45, 46]. In particular, and motivated by experimental setups, we explore deformations of such a free interface and their coupling with domain nucleations as induced by different surface chemical patterings.

In order to change the balance between energies associated with bending and modulations and allow deformations of the free interface, we consider specifically the case where the segregation in ρ is weak but that of ϕ is still strong. This is done by choosing $\tau = 1.8$, $\chi = 4.1$ and $\mu_\rho = -0.101682$ (and $\mu_\phi = 0$ for symmetric lamellae), while recalling that the critical point values for $\rho = 1$ are given by $\tau_c = 1$ and $\chi_c = 4$. The effect of surface-induced modulation on a weakly-segregated interface is seen in figure 10, where the lower surface is chosen to have the following step pattern:

$$\sigma_\phi = \begin{cases} -0.1 & 0 \leq x \leq 4d_0 \\ 0.1 & -4d_0 \leq x \leq 0 \end{cases} \quad (26)$$

and $\sigma_\rho = 0$ for the entire substrate. This patterning causes a defect formation at the mid-point $x = 0$, where the change in σ_ϕ occurs. The defect, in turn, induces a deformation of the solvent/polymer (free) interface, forming several terraces. The jumps in terrace height is about half of the lamellar periodicity, in agreement with previous results obtained using self-consistent field theory (SCFT) [24].

A defect can also be obtained between L_{\perp} and $L_{||}$ lamellar phases by choosing a patterned substrate that prefers an $L_{||}$ in its mid-section and an L_{\perp} elsewhere:

$$\sigma_\phi = \begin{cases} 0.1 & |x| \leq 2d_0 \\ 0 & 4d_0 > |x| > 2d_0 \end{cases} \quad (27)$$

and $\sigma_\rho = 0$ for the entire substrate. As can be seen in figure 11, this surface pattern causes a deformation of the free interface between the BCP (lamellar) and solvent phases. In the mid-section, $L_{||}$ has a thickness of three layers ($y \approx 1.5d_0$), and a terrace then separates the mid-section $L_{||}$ from the side ones where the L_{\perp} is

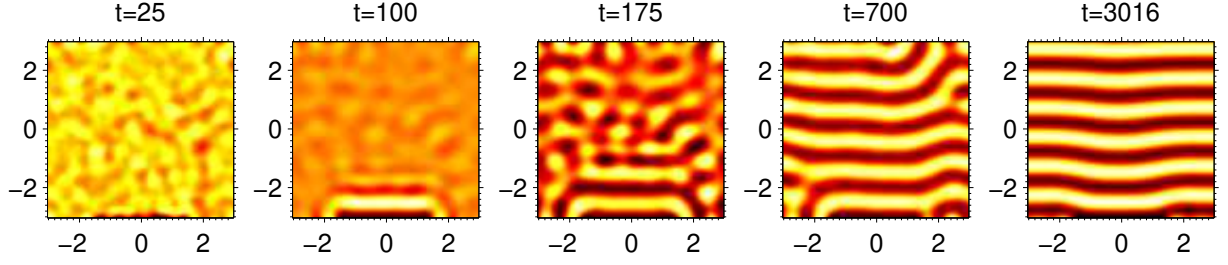


FIG. 9: (colored online) Temporal evolution of the order parameter ϕ for a symmetric bulk lamellar phase, $\phi_0 = 0$. The time step t measures the number of numerical iterations and progresses from left to right: $t = 25, 100, 175, 700$ and 3016 .

We set periodic boundary conditions on the side walls, while the central section of the lower surface prefers the B-component, $\sigma_\phi = 0.5$ for $-1.5d_0 \leq x \leq 1.5d_0$ and is zero elsewhere, as in eq 25. A nucleation of a distorted L_{\parallel} phase starts at $t \gtrsim 100$ and then propagates into the bulk. The axes are given in units of $d_0 = 2\pi/q_0$, and the color bar accounts for variation of each order parameter. The patterns are produced using eq 5 with $\chi = 5.5$, $\tau = 1.2$

$\mu_\rho = -0.004236$, $\mu_\phi = 0$, $H = K = 1$ and $q_0 = 1/\sqrt{2}$, for which the lamellar phase the equilibrium one.

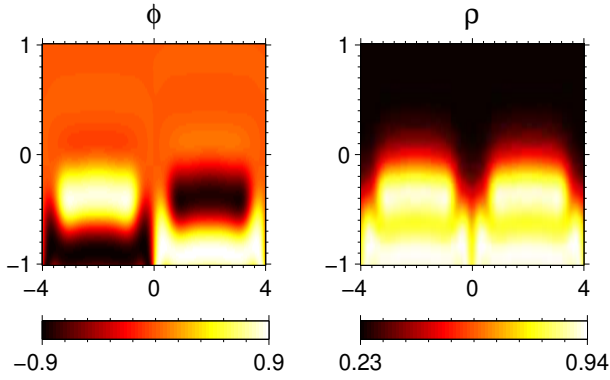


FIG. 10: (colored online) Terrace formation both in ϕ (left) and ρ (right) for a lamellar structure due to patterned substrate as in eq 26. The system is at its solvent-lamellar coexistence with $\tau = 1.8$, $\chi = 4.1$, $\mu_\rho = -0.101682$ and $\mu_\phi = 0$, leading to bulk volume fractions of $\phi_A = \phi_B = 0.245$ and $\phi_S = 0.51$ ($\phi = 0$ and $\rho = 0.49$). The axes are given in units of $d_0 = 2\pi/q_0$, and the color bar accounts for variation of each order parameter.

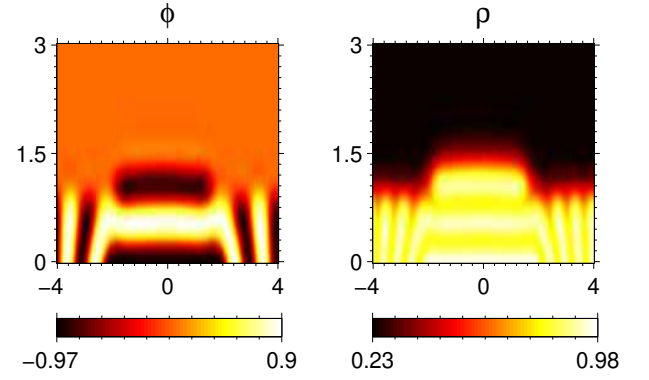


FIG. 11: (colored online) Parallel (L_{\parallel}) and perpendicular (L_{\perp}) domains in equilibrium with a pure solvent phase ($\sigma_\rho = 0$) in presence of a surface pattern as in eq 27.

Terrace formation and deformation of the free (solvent/BCP film) interface can be seen. The system parameters are: $\tau = 1.8$, $\chi = 4.1$, $\mu_\rho = -0.101682$ and $\mu_\phi = 0$, corresponding to a slightly asymmetric lamellar phase with $\phi_A = 0.23$, $\phi_B = 0.246$ and $\phi_S = 0.524$. The axes are given in units of $d_0 = 2\pi/q_0$, and the color bar accounts for variation of each order parameter.

the preferred orientation. Moreover, the L_{\perp} phase is deformed and tilted at the boundary with the L_{\parallel} phase, and the width of this boundary increases as τ approaches its critical value.

Another way of deforming the free interface is to induce a BCP droplet by a patterned substrate in coexistence with the solvent phase. For that purpose the substrate is separated into a central section that prefers the BCP with $\sigma_\rho < 0$ (wetting condition), while on the rest of the surface $\sigma_\rho > 0$, which repels the lamellar phase (non-wetting condition that prefers the solvent). In addition, by manipulation the σ_ϕ field, we can induce different do-

main inside the same droplet.

$$\sigma_\rho = \begin{cases} -0.5 & |x| \leq 5d_0 \\ 0.5 & 6d_0 > |x| > 5d_0 \end{cases}$$

$$\sigma_\phi = \begin{cases} 0.5 & |x| \leq d_0 \\ 0 & 6d_0 > |x| > d_0 \end{cases} \quad (28)$$

Such a case in which both L_{\perp} and L_{\parallel} domains co-exist within the same BCP droplet is shown in figure 12. The patterning leads to central domain of the droplet in the L_{\parallel} orientation surrounded by two deformed L_{\perp} domains

that compensate between the height of the L_{\parallel} phase and the edges of the droplet.

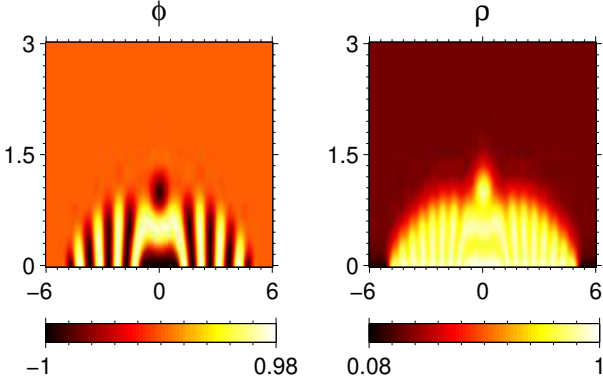


FIG. 12: (colored online) A BCP lamellar droplet wetting a substrate. The wetting is formed using a surface field that attracts the BCP to its mid-section and repels it elsewhere, as in eq 28. Domains of different orientations are further induced inside the lamellar droplet by a σ_{ϕ} surface field [eq 28]. The lamellar/solvent phase coexistence occurs for $\tau = 1.8$, $\chi = 4.1$, $\mu_{\phi} = 0$ and $\mu_{\rho} = 0$, corresponding to $\phi_A = 0.187$, $\phi_B = 0.183$ and $\phi_S = 0.629$. The axes are given in units of $d_0 = 2\pi/q_0$, and the color bar accounts for variation of each order parameter.

The morphologies found in this section result from substrate patterning, and are in agreement with the ones obtained recently using a more computationally intensive method of SCFT [24]. One drawback of our numerical minimization scheme is that the BCP volume fraction is not a conserved quantity. We partially overcome this difficulty by working in the weak-separation regime between the BCP and a bad solvent. These results describe long-lived metastable states that are not the full thermodynamically equilibrated structures. They enable us to observe qualitatively how such a deformed free interface is created, but do not give any quantitative conclusion regarding the free interface at full thermodynamic equilibrium.

VI. SURFACE TENSION AND DOMAIN SHAPE OF LAMELLAR PHASES

As seen in the preceding sections, our model describes different types of coexisting phases and their interfaces. We proceed by analyzing the surface tension between a solute-rich lamellar phase and a solvent-rich disordered phase as function of the phase separation controlling parameters: τ and χ . A schematic illustration of the two coexisting phases is shown in figure 13, and our calculations are performed for 2d systems of volume $V = L_x \times L_y$. The surface tension between any two coexisting phases (I and II), is defined as $\gamma = [G^{I,II}(V, A) - \frac{V}{2}(g_b^I + g_b^{II})]/A$, where $A = L_x$ is the projected area of the interfacial layer, and

for convenience, each of the two phases occupies half of the total volume.

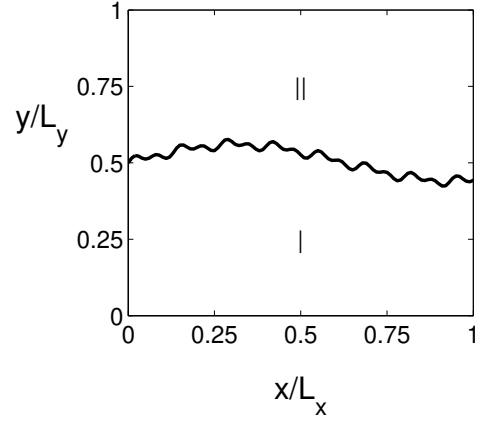


FIG. 13: Schematic drawing of an undulating interface separating two coexisting phases. The bottom one is denoted by 'I' and the top one by 'II'. The 2d system volume is $V = L_x \times L_y$ and the interface projected area is $A = L_x$.

Coexistence between the two phases is achieved by tuning the appropriate chemical potentials. The free energy G^I of a lamellar BCP phase of volume $V/2$ is calculated numerically by imposing periodic boundary conditions on the side boundaries and free boundary conditions on the upper and lower surfaces. The distance between upper and lower surfaces of the box, L_y , is adjusted so that the free energy G^I is minimized. This occurs when L_y is an integer multiple of the modulated periodicity. Therefore, G^I corresponds to a phase with no defects with a free energy density $g_b^I = G^I/(V/2)$. The same procedure is used to calculate the bulk free energy of the disordered phase, $g_b^{II} = G^{II}/(V/2)$. This procedure is repeated until we find the chemical potential yielding two coexisting phases with $g_b^I = g_b^{II}$. When the simulation box V is big enough and for the proper chemical potentials, an initial guess of an upper phase (phase I) and a lower one (phase II) will converge into two coexisting phases with an interface in between them.

We would like to compare the surface tension between a symmetrical lamellar phase ($\phi = 0$) and a solvent one where the lamellae meet the L-S interface at different angles. By choosing proper initial conditions we consider two limiting orientations: lamellae that are parallel to the interface (L_{\parallel}), and those that are perpendicular (L_{\perp}). The corresponding surface tension, γ_{\parallel} and γ_{\perp} , is then computed as function of τ for $\chi = 4.5$ and plotted on figure 14. Three distinctive regions can be observed from the figure. For $\tau < \tau_c$ the solute phase is disordered (D) and changes into a lamellar phase (L) only above τ_c . It then turns back into a disordered phase (D) for $\tau > \tau_{tri}$, where τ_{tri} is the triple point. Namely, only in the range $\tau_c \leq \tau \leq \tau_{tri}$, the lamellar phase exists and the two orientations, L_{\parallel} and L_{\perp} , can be compared. This is

in agreement with the studies of ref [12] along the $\phi = 0$ line. Numerically, we find $\tau_c \simeq 1.29$, and for $\tau < \tau_c$ the solute-rich phase is disordered ($\phi = 0$) with a finite value of ρ . Since $\phi_0 = 0$, the free energy of eq 5 does not depend on τ , and the surface tension for the S - D coexistence is constant.

In the region of $\tau > \tau_c$, the lamellar phase is energetically favored over the D phase, and the change in the surface tension is in agreement with an S - L coexistence. Furthermore, above τ_c , the segregation between the A/B components grows, causing the lamellae to grow in magnitude and increases the change in density at the S - L interface, thus causing the two surface tensions, γ_{\parallel} and γ_{\perp} , to increase.

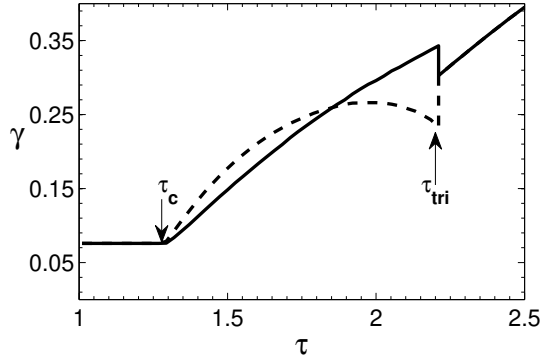


FIG. 14: Surface tensions, γ_{\parallel} and γ_{\perp} , for the Lamellar-Solvent interface for two lamellar orientations, parallel (dashed line) and perpendicular (solid line), as function of τ for fixed $\chi = 4.5$. The lamellar phase exists only inside the interval $\tau_c < \tau < \tau_{\text{tri}}$. Elsewhere the surface tension is between a disordered liquid (D) and a solvent phase (S). Up to a crossover $\tau^* \simeq 1.848$, γ_{\perp} (solid line) has a lower value than γ_{\parallel} (dashed line), and the perpendicular lamellae are preferred. While for $\tau > \tau^*$, $\gamma_{\perp} > \gamma_{\parallel}$ and L_{\parallel} is preferred. At τ_{tri} there is a first-order phase transition and hence the jump there in γ .

It is worth noticing that γ_{\perp} is a monotonically increasing function of τ while γ_{\parallel} is non-monotonic. However, while the segregation between the A and B component grows, the modulation amplitude reaches saturation, $\phi_q \rightarrow 1$, causing the width of the boundary between A and B to diminish. Eventually, as τ increases even further, another jump in surface tension appears at the triple point ($\tau_{\text{tri}} \simeq 2.215$), where the lamellar phase is no longer favored, and the disordered phase takes over via a first-order phase transition. As $\phi \neq 0$, it gives a τ -dependent behavior of γ due to the $\tau\phi^2$ term in the free energy.

Comparing the two orientations of the lamellar phase, it is seen that for low values of τ , the transverse orientation is preferred at the interface, while for larger τ values, L_{\parallel} is the preferred one. The crossover occurs at $\tau^* \simeq 1.848$ and indicates that the mere existence of the solvent interface may induce a preferred direction of bulk

modulations. This result implies that by incorporating steric repulsion (in which $\phi = \rho = 0$ on any of the confining surfaces), the L_{\parallel} phase is preferred next to any neutral surface for large τ values.

Because the γ_{\perp} and γ_{\parallel} have very different dependence on τ , one might expect to see that an initial round droplet containing a lamellar BCP becomes oval. For example, by choosing $\tau = 1.6 < \tau^*$, $\chi = 4.5$ and a chemical potential at coexistence, $\mu_{\rho} = -0.058629$, $\gamma_{\perp} < \gamma_{\parallel}$ causes the L_{\parallel} - S interface to reduce its length, while the L_{\perp} - S compensates and increases its length. As has been already commented, the conservation of $\langle \rho \rangle$ is problematic within our numerical scheme. We can, nevertheless, look at a droplet which is set to be initially circular and observe how it deforms while diminishing in size. This is seen in figure 15. At $t = 1$ [figure 15(a)], the droplet is circular and the lamellae are preset to orient vertically. At progressive time steps, the lamellae orientation deforms so that the lamellae meet the interface at a right angle. While the droplet diminishes in size, it does not diminish uniformly. Because the parallel boundary diminishes faster ($\gamma_{\perp} < \gamma_{\parallel}$), the droplet undergoes a continuous shape change, giving the droplet a biconvex lentil-shape at later time steps [figure 15(d)]. If we continue the simulations even further, the droplet will eventually disappear, because our numerical scheme does not conserve the ρ order parameter.

We would like to compare our findings with experimental ones. Formation of lens-like BCP macro-domains embedded in a solvent matrix during solvent/polymer phase separation was observed experimentally [47] for blends of poly(styrene-block-isoprene) and homopolystyrene acting as a bad solvent. The relationship between the macro-phase separation (solvent/BCP) and the self-assembly of the BCP inside the domains was reported and analyzed. Although we cannot offer a direct explanation of these experiments because our model is restricted to study lamellae in two dimensions, while in Ref. [47] cylindrical phases of BCP are studied in three dimensions, the resemblance of our Fig. 15 with Fig. 5 of Ref. [47] is striking, and may be regarded as 2d cuts through the 3d cylindrical BCP domain. We note that in Ref. [47] a similar explanation for the creation of lens-like domains with orientation of the cylinders along the smaller lens axis was given, and is consistent with a difference in surface tension between the two orientations, $\gamma_{\perp} < \gamma_{\parallel}$.

More recently, addition of Au-based surfactant nanoparticles led to change in shape and morphology for particles based on poly(styrene-b-2-vinylpyridine) diblock copolymers [48]. The added nanoparticles are adsorbed at the interface between block copolymer-containing droplets and the surrounding amphiphilic surfactant. In turn, it causes a preferred perpendicular orientation of the BCP lamellae and led to distortion of the BCP droplets into ellipsoid-shaped ones. The system is more complex as it includes an additional component, but the explanation presented by the authors for the distorted shape is similar to ours and relies on the

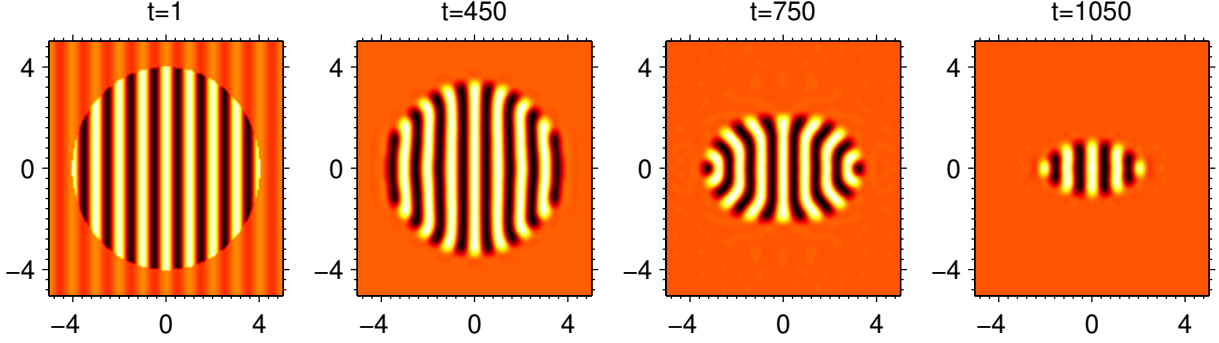


FIG. 15: (colored online) The temporal evolution of the ϕ order parameter of a lamellar BCP droplet in coexistence with a solvent phase. From left to right: $t = 1, 450, 750$ and 1050 , where the time step t measures the number of numerical iterations. The parameters used are $\tau = 1.6$, $\chi = 4.5$, $\mu_\rho = -0.058629$, and $\mu_\phi = 0$. As the BCP droplet volume is not constrained to stay constant, because of surface tension the droplet diminishes in size until it vanishes. The surface tension is anisotropic because the lamellae meet the droplet interface with different angles. It causes the original circular droplet to deform into a biconvex lens-shape, which is preferred energetically. The axes are given in units of $d_0 = 2\pi/q_0$, and the color bar accounts for variation of each order parameter.

anisotropic surface tension as enhanced by the added Au nanoparticles.

In another study [49], lamellar domain formation has been reported following a temperature quench from a disordered BCP phase to the lamellar one. The formed lamellar domains are lens-shaped with their axes along the smaller domain axis. It might of interest to see if a large change in the final temperature of quenching may cause the formation of lens domains with parallel-oriented lamellae, as is predicted by our study, where γ_\perp and γ_\parallel have different (and non-monotonous) temperature dependence.

VII. CONCLUSIONS

In this paper, we investigate bulk properties of solvent-diluted BCP phases, and a variety of interfaces between coexisting BCP and solvent phases, restricting ourselves to phases with 1d (lamellar) and 2d (hexagonal) morphologies. The main assumption made is the dominant nature of a single q_0 mode, which allows us to write a simplified mean-field form of the free energy. Although the dominant q_0 -mode can be justified in the weak-segregation limit, we believe that many of the reported results are qualitatively correct also at stronger segregation.

To further simplify the model, the numerical investigations are conducted for the case where the interactions between the A and B monomers of the BCP and the solvent (S) are identical. Namely, there is no bilinear enthalpic term as $\phi\rho$ in the free energy ($v_{\phi\rho} = 0$). Hence, the coupling between the two order parameters, ϕ and ρ , originates only from entropy of mixing and is even in ρ . Its leading order is $\phi^2\rho$. The global phase diagrams (figure 1) are obtained by a numerical minimization of the free energy, for different values of the two interaction

parameters, τ and χ . The diagrams display a variety of phases such as Disorder (D), Lamellar (L), Hexagonal (H) and Solvent (S). The phase behavior contains also two- and three-phase coexistence regions bounded by critical points.

The coupling between ρ , the volume fraction of the solute, and ϕ , the BCP relative A/B composition leads to two interesting analytical results valid in the low solvent limit, $\rho \approx 1$. First, the critical point τ_c that determines the onset of BCP phases becomes ρ dependent, $\tau_c = 1/\rho$. Second, due to the non-linear nature of the coupling, modulations in ϕ induce modulations in ρ , with a doubled wavenumber, as was explained in detail in section III.C. This phenomenon also results in formation of density bulbs at the interface between a modulated BCP and a disordered phase (figures 6 and 7), and a “star of David” formation in an hexagonal phase (figure 8), which decay at the BCP/solvent interface and into the disorder solvent phase.

It is of interest to remark on the rotational-symmetry breaking of BCP domains at the BCP/solvent coexistence. We found that the surface tension of the parallel phase (γ_\parallel) is higher than that of the transverse phase (γ_\perp) for small values of τ , while the opposite occurs for large τ values. This crossover causes a BCP lamellar to change its orientation relative to the interface as one changes τ , and should be taken into consideration, as it may be used to induce some preferred direction or interfere with such an attempt. This difference in surface tension causes modulated droplets to deform. Although this result is relevant to strong ϕ segregation while our model is accurate next to the critical point, we believe that it represents a general phenomenon that can be applied to other situations, such as the shape of domains composed of a hexagonal BCP phase coexisting with a solvent phase.

Acknowledgements. We thank H. Orland and

X.-K. Man for many useful discussions. This work was supported in part by the Israel Science Foundation under grant no. 438/12.

Appendix A: Numerical Details

The conjugate gradient (CG) method is a numerical algorithm designed to find a local minimum of a smooth, multi-dimensional nonlinear function [50]. In our case it was applied to minimize the Ginzburg-Landau free-energy expansion, given in eq 5.

We used a discrete $L_x \times L_y$ simulation box where the order parameters ϕ and ρ depend on the discrete lattice points (x_i, y_j) . The total energy is calculated as a sum over all sites, where the differences between the order parameter in one site and the other is used to estimate the derivatives using their discrete form while penalty functions are used to avoid non-physical values of the order parameters.

Two types of boundary conditions are given to the

solver. The first are periodic boundary conditions used for simulating bulk behavior. In the second one the free energy is coupled to some surface pattern (e.g., a surface patterned field).

As our model and dynamics do not include random fluctuations, the initial guess of the order parameters, ϕ and ρ , plays an important role. In some cases a random initial guess is used to make the solver converge to the absolute minimum (which is very time demanding), while in most cases several well chosen initial guesses are used to speed convergence, especially when it is applied to model the interface between two coexisting phases.

When the thermodynamics dictates that only one phase is at thermodynamical equilibrium, the average value of the order parameters can be adjusted by changing the chemical potential related to them. In a coexistence region of two (or more) phases defined by setting the chemical potentials to their proper values, the total amount of each species is not conserved during the numerical iterations of the CG algorithm.

-
- [1] M. Seul and D. Andelman, *Science* **267**, 476 (1995).
 - [2] D. Andelman and R. E. Rosensweig, in *Polymers, Liquids and Colloids in Electric Fields: Interfacial Instabilities, Orientation, and Phase-Transitions*, Ed. by Y. Tsori and U. Steiner, Vol. 2 in *Series in Soft Condensed Matter* (World Scientific, Singapore, 2009), chapter 1, pp. 1-56.
 - [3] D. Andelman and R. E. Rosensweig, *J. Phys. Chem. B* **113**, 3785 (2009).
 - [4] S. Leibler and D. Andelman, *J. Phys. (France)* **48**, 2013 (1987).
 - [5] M. Plischke and B. Bergersen, *Equilibrium Statistical Physics* (World Scientific, Singapore, 2006).
 - [6] S. A. Brazovskii, *Sov. Phys. JETP* **41**, 85 (1975).
 - [7] L. Leibler, *Macromolecules* **13**, 1602 (1980).
 - [8] G. H. Fredrickson and E. Helfand, *J. Chem. Phys.* **87**, 697 (1987).
 - [9] G. H. Fredrickson and K. Binder, *J. Chem. Phys.* **91**, 7265 (1989).
 - [10] I. W. Hamley and V. E. Podnests, *Macromolecules* **30**, 3701 (1997).
 - [11] Y. Tsori and D. Andelman, *Macromolecules* **34**, 2719 (2001).
 - [12] R. R. Netz, D. Andelman and M. Schick, *Phys. Rev. Lett.* **79**, 1058 (1997).
 - [13] D. Andelman, F. Brochard and J. F. Joanny, *J. Chem. Phys.* **86**, 3673 (1987).
 - [14] Y. Tsori, D. Andelman and M. Schick, *Phys. Rev. E* **61**, 2848 (2000).
 - [15] G. Fredrickson, *Macromolecules* **20**, 2535 (1987).
 - [16] Y. Tsori and D. Andelman, *Europhys. Lett.* **53**, 722 (2001).
 - [17] Y. Tsori and D. Andelman, *Eur. Phys. J. E* **5**, 605 (2001).
 - [18] Y. Tsori and D. Andelman, *Macromolecules* **38**, 7193 (2005).
 - [19] Y. Tsori and D. Andelman, *Macromolecules* **36**, 8560 (2003).
 - [20] A. K. Khandpur, S. Foerster, F. S. Bates, I. W. Hamley, A. J. Ryan, W. Bras, K. Almdal and K. Mortensen, *Macromolecules* **28**, 8796 (1995).
 - [21] S. P. Gido, J. Gunther, E. L. Thomas and D. Hoffman, *Macromolecules* **26**, 4506 (1993).
 - [22] S. P. Gido and E. L. Thomas, *Macromolecules* **27**, 6137 (1994).
 - [23] T. Hashimoto, S. Koizumi and H. Hasegawa, *Macromolecules* **27**, 1562 (1993).
 - [24] X. K. Man, D. Andelman and H. Orland, *Phys. Rev. E* **86**, 010801, (2012).
 - [25] G. Coulon, T. P. Russell, and V. R. Deline, *Macromolecules*, **22**, 2581 (1989).
 - [26] A. Knoll, A. Horvat, K. S. Lyakhova, G. Krausch, G. J. A. Sevink, A. V. Zvelindovsky, and R. Magerle, *Phys. Rev. Lett.* **89**, 035501 (2002).
 - [27] A. Knoll, R. Magerle, and G. Krausch, *J. Chem. Phys.* **120**, 1105 (2004).
 - [28] M. Stoykovich, M. Müller, S. Kim, H. Solak, E. Edwards, J. J. de Pablo, and P. F. Nealey, *Science* **308**, 1442 (2005).
 - [29] R. Ruiz, H. M. Kang, F. A. Detcheverry, E. Dobisz, D. S. Kercher, T. R. Albrecht, J. J. de Pablo, and P. F. Nealey, *Science* **321**, 936 (2008).
 - [30] J. Bang, U. Jeong, D. Y. Ryu, T. P. Russell, and C. J. Hawker, *Adv. Mater.* **21**, 4769 (2009).
 - [31] R. Segalman, H. Yokoyama, and E. J. Kramer, *Adv. Mater.* **13**, 1152 (2001).
 - [32] G. E. Stein, W. B. Lee, G. H. Fredrickson, E. J. Kramer, X. Li, and J. Wang, *Macromolecules* **40**, 5791 (2007).
 - [33] H.-W. Li, and W. T. S. Huck, *Nano Lett.* **4**, 1633 (2004).
 - [34] V. Voet, T. Pick, S.-M. Park, M. Moritz, A. Hammack, D. Urban, D. Ogletree, D. Olynick, and B. Helm, *J. Am. Chem. Soc.* **133**, 2812 (2011).
 - [35] P. Thebault, S. Niedermayer, S. Landis, N. Chaix, P. Guenoun, J. Daillant, X. K. Man, D. Andelman, and H.

- Orland, Adv. Mater. **24**, 1952 (2012).
- [36] M. Rubinstein and R. H. Colby, *Polymer Physics* (Oxford University, N.Y, 2003).
- [37] M. Doi, *Introduction to Polymer Physics* (Oxford University, Oxford, 1996).
- [38] S. Safran, *Statistical Thermodynamics of Surfaces, Interfaces, and Membranes* (Frontiers in Physics, MA, 1997).
- [39] T. Garel and S. Doniach, Phys. Rev. B **26**, 325 (1982).
- [40] T. Ohta and K. Kawasaki, Macromolecules **19**, 2621 (1986).
- [41] S. Villain-Guillot and D. Andelman, Eur. Phys. J. B **4**, 95 (1998).
- [42] S. Villain-Guillot, R. R. Netz, D. Andelman and M. Schick, Physica A **249**, 284 (1998).
- [43] Note that if we include the asymmetric $v_{\phi\rho}$ term in eq 5, this will add a 1st harmonic term in the expansion of $\eta(x)$ of the form: $\eta_q \cos(q_0 x)$ with $\eta_q = 2v_{\phi\rho}\phi_q/(4Kq_0^2 + \varepsilon)$
- [44] E. Burgaz and S. P. Gido, Macromolecules **33**, 8739 (2000)
- [45] M. W. Matsen, J. Chem. Phys. **106**, 7781 (1997).
- [46] P. Stasiak, J. D. McGraw, K. Dalnoki-Veress, and M. W. Matsen, Macromolecules **45**, 9531 (2012).
- [47] S. Koizumi, H. Hasegawa, and T. Hashimoto, Macromolecules **27**, 6532 (1994).
- [48] S. G. Jang, D. J. Audus, D. Klinger, D. V. Krogstad, B. J. Kim, A. Cameron, S.-W. Kim, K. T. Delaney, S.-M. Hur, K. L. Killops, G. H. Fredrickson, E. J. Kramer and C. J. Hawker, J. Am. Chem. Soc. **135**, 6649 (2013).
- [49] T. Hashimoto, N. Sakamoto and T. Koga, Phys. Rev. E. **54**, 5832 (1996).
- [50] W. H. Press, S. A. Teukolsky, W. T. Vetterling and B. P. Flannery, *Numerical Recipes* (Cambridge University, N.Y, 1992).